ROYAL SOCIETY
OF CHEMISTRY

PAPER

Check for updates

Polymeric nanoparticles based on carboxymethyl chitosan in combination with painless microneedle therapy systems for enhancing transdermal insulin delivery

Pei Zhang, [ID][a] Yan Zhang[a] and Chen-Guang Liu*[b]

Biodegradable nanoparticles (NPs) have been frequently used as insulin transdermal delivery vehicles due to their grand bioavailability, better encapsulation, controlled release and less toxic properties. However, the skin's barrier properties prevent insulin-loaded NP permeation at useful levels. Nowadays, microneedles have been spotlighted as novel transdermal delivery systems due to their advantages such as painlessness, efficient penetration and no hazardous residues. Herein, we introduce polymeric nanocarriers based on carboxymethyl chitosan (CMCS) for insulin delivery, combining with microneedle therapy systems, which can rapidly deliver insulin (INS) into the skin. The resulting CMCS-based nanocarriers are spherical nanoparticles with a mean size around 200 nm, which could generate supramolecular micelles to effectively encapsulate insulin (EE% = $83.78 \pm 3.73\%$). A nanocrystalline microneedle array (6×6, 75/150 μm) was used to penetrate the stratum corneum (SC) for enhancing transdermal insulin delivery, while minimizing the pain sensation caused by intravenous injection. Compared with the transdermal rate of passive diffusion [2.77 ± 0.64 μg (cm^{-2} h^{-1})], the transdermal rate of the insulin-loaded NP combined with microneedle penetration shows a 4.2-fold increase [10.24 ± 1.06 μg (cm^{-2} h^{-1})] from permeation experiment *in vitro*. *In vivo* hypoglycemic experiments demonstrate the potential of using nanocarrier combination with microneedle arrays for painless insulin delivery through the skin in a clinical setting. Thus, the developed combination scheme of nanoparticles and microneedle arrays offers an effective, user-friendly, and low-toxicity option for diabetes patients requiring long-term and multiple treatments.

1. Introduction

As of 2019, 463 million people suffered from diabetes worldwide and the total number of people with diabetes is estimated to rise to 642 million by 2045.[1–3] Diabetes mellitus are a group of metabolic diseases characterized by the failure of blood glucose level regulation mechanisms.[4,5] Poor blood glucose control may also increase the progression of microvascular diseases, kidney failure and the risk of heart attacks, and impaired blood glucose level regulation mechanisms.[6,7] The traditional care for patients with type 2 diabetes often requires monitoring of blood glucose levels and insulin therapy to maintain normoglycemia.[8,9] However, such self-administration is associated with pain and it requires injections over his or her lifetime.[10,11] Various alternative routes of non-injectable insulin delivery including rectal, intrapulmonary, oral, ocular, nasal, buccal and dermal have thus been considered for the administration of insulin.[12–16] The

noninvasive transdermal route, in particular, is an attractive candidate for the steady and sustained delivery of insulin into the blood in a pain-free manner, which minimizes and circumvents the limitations associated with the oral, parenteral, and inhalation methods of drug administration.[17] In addition, the main advantages of the transdermal routes are low proteolytic activity of the skin and the possibility of continuously delivering drugs with short half-lives and prolonged effects by continuous absorption, avoidance of drug level fluctuation and ease of drug delivery termination in the occurrence of toxicity.[18,19] However, transdermal delivery systems (TDDSs) also faces major challenges in circumventing the barrier function of the outermost layer of the skin, the stratum corneum (SC), which works against drug penetration into the skin and the systemic drug circulation.[20,21] Developing new solutions for penetrating the SC is necessary to solve the problem in insulin transdermal delivery; one such solution has been the micronization of drug particles.[22]

Self-assembled nanoparticles such as liposomes and polymeric NPs are designed to maintain the physicochemical properties of the encapsulated insulin and facilitate

[a]*Department of Life Science, Luoyang Normal University, Luoyang 471934, PR China*
[b]*College of Marine Life Sciences, Ocean University of China, Qingdao 266003, PR China. E-mail: liucg@ouc.edu.cn; Fax: +86 532 82032586; Tel: +86 532 82032102*

transdermal delivery.[23,24] Specially, polysaccharide-based self-assembled nanostructures composed of an inner hydrophobic core and an outer shell of hydrophilic groups are one of the potential nanocarriers to deliver drug for their good biocompatibility and natural degradation/resorption pathways.[25] The insulin-loaded NPs typically have two major advantages as a therapeutic option for transdermal delivery, namely, (i) high drug loading:[26] this property is primarily ascribable to the unique amphiphilic structure, which, upon self-assembly, results in NPs with more, low-density hydrophobic cores able to accommodate a substantial amount of insulin; (ii) small micellar size with narrow size distribution: such small-sized nanoparticles favor deeper penetration into cells and concurrently prolong the beneficial accumulation times in cells *via* sustained release.[27] In addition, attention has been paid to the possibility of using microneedles (MNs) in delivering insulin into the skin.[28] As a novel and minimally invasive delivery system, MNs are capable of creating transient aqueous microchannels across the skin for small-molecule drugs, therapeutic proteins, or nanoparticles to achieve enhanced transdermal drug delivery.[29,30] Compared with the device of injections, a microneedle should be large enough to penetrate the stratum corneum and provide precise penetration deeply under the skin by controlling the length of the needles, but still be small enough to reduce the damage to skin nerves and pain, and also avoid the need for expert training to administer.[31–33] Thus far, the solid microneedles have been proved to be an efficient and affordable approach for the precise skin localization of insulin delivery with minimal invasiveness.[34] For instance, a short length of the silicon microneedle was able to pierce the mouse skin with the help of an electric applicator.[35]

Inspired by these unique features of these delivery devices, we linked hydrophobic conjugated linoleic acid (CLA) to CMCS molecules with the intention to form amphiphilic CLA–CMCS (CC), which can be used as a protein-based nanocage. Furthermore, a hydrophilic functional amino acid chain (arginine, Arg), which has been extensively studied as a cell-penetrating peptide that mediates the cell binding and trans-epithelial transport, was grafted to a CC block copolymer by amide bonding to form a CLA–CMCS–Arg (CCA) polymer.[36] Then, we prepared CC/CCA-NPs that possess a large amount of hydrophobic cores and penetration factors might be able to achieve both excellent drug encapsulation and transdermal delivery. In addition, to achieve optimal efficiency of skin penetration, four NPs with different surface ligands (CC-NPs and CCA-NPs) and two different lengths of microneedles (needle length: 75 and 150 μm) were combined and systemically investigated. We demonstrated a strong correlation between the length of microneedles and the completely different penetration efficiency. CCA-NPs exhibited both excellent encapsulation efficiency and satisfactory skin penetration efficiency when combined with microneedles with a longer needle length (150 μm). This method combines the controlled release properties of nanocarriers with the efficacy of conventional injection needles, while minimizing the disadvantages of these administration methods.[37] To demonstrate the feasibility of this combination method for protein drug delivery *in vivo*, we further investigated the therapeutic efficacy of insulin-loaded NPs following transdermal delivery.

2. Materials and methods

2.1 Materials

Carboxymethyl chitosan (CMCS, MW = 10 kDa, substitution degree of carboxymethyl >80%) was obtained from Honghai Biotechnology Co., Ltd. (Tsingtao, China). L-Arg was purchased from HuiXing Biochemistry Reagent Co., Ltd. (Beijing, China). Conjugated linoleic acid (CLA) and a glucose assay kit were obtained from Solarbio (Shanghai, China). A dialysis bag (MW$_{CO}$ = 7000 Da), insulin (INS), streptozotocin (STZ), sodium pentobarbital and other biomedical applications were obtained from Sigma (New York, USA). All other reagents were of analytical grade and used without further purification. Nano-microneedle: the solid nano-microneedle used in this study consists of a microneedle array chip attached to a plastic crystal head, and this was provided by Natong Bio-Nano Technology Co., Ltd. (Suzhou, China).[38]

2.2 Fabrication and characterization of self-assembled nanoparticles of CC/CCA conjugates

The CC/CCA conjugates were prepared by a reported method with hydrophobic and functional modifications, and then suspended in distilled water at 37 °C for 24 h.[39] The solution was then sonicated three times using a probe-type sonifier (UR-200P, Tomy Seiko, Japan) at 90 W for 2 min each, in which the pulse was turned off for 3.0 s with an interval of 5.0 s to prevent the increase in temperature. The morphological examination of CC/CCA-NPs was conducted by TEM (H-600A, Hitachi, Japan). The samples were diluted with water and placed on copper grids, which were air-dried and negatively stained with 1% (W/V) phosphotungstic acid prior to the observation. The CC/CCA-NPs were dispersed in 0.2 M phosphate buffered solution (PBS, pH 7.4) and sonicated to determine the particle size, polydispersity (PDI), and zeta potential using a Malvern Zetasizer (3000HSA, Malvern, UK) at 25 °C.

2.3 Cell compatibility assay of CC/CCA-NPs

Cell cytotoxicity of CC/CCA-NPs was determined by an MTT assay.[36] L929 cells at a density of 4×10^5 cells per mL were seeded into 96-well plates and allowed to adhere. The culture medium was replaced with a new complete medium containing blank CC/CCA-NPs at final concentrations of 250–2000 μg mL^{-1}. The cells were incubated at 37 °C for 24 h. After pre-determined incubation, the MTT solution was added to each well. After 4 h of incubation at 37 °C, the medium was removed and any formazan crystals formed were solubilized with DMSO. After slowly shaking for 10 min, the absorbance of each well was determined at 490 nm using a microplate reader. The cell viability was expressed in percentage compared to the control (only test cells were added).

2.4 Preparation of insulin-loaded CC/CCA-NPs

The CC/CCA-NPs was used to encapsulate insulin *via* hydrophobic interaction.[40] Briefly, insulin (27.9 IU mg^{-1}) was dissolved in a PBS solution (pH = 7.4) to form the insulin stock solution, achieving concentrations of 4 mg mL^{-1}. Then, 1 mL insulin solution was mixed with 4 mg of different NPs (CC and CCA) in 4.0 mL PBS buffer (10 mM, pH 7.4) and immediately vortexed for 15–30 s. Then, the mixture was incubated at room temperature for 20–30 min under stirring, to completely form insulin-loaded NPs. Non-encapsulated insulin was separated by dialysis for 9 h (changing water every hour) using a dialysis bag with a molecular weight cutoff of 7000 Da. The product in the dialysis bag was subsequently lyophilized. Insulin was measured by high-performance liquid chromatography (HPLC, Agilent 1100, USA). The drug-loading content and drug encapsulation efficiency were calculated as follows:

$$\text{Drug loading content (\%)} = W_t/W_s \times 100\% \tag{1}$$

$$\text{Encapsulation efficiency (\%)} = W_t/W_o \times 100\% \tag{2}$$

W_t represents the amount of insulin loaded into nanoparticles, W_o the initial amount of insulin fed, and W_s the amount of nanoparticles after lyophilization.[41]

2.5 *In vitro* permeation studies

2.5.1 Rat skin. Male Sprague-Dawley (SD) rats weighing 200 ± 20 g were obtained from the Institute for Port Drug Inspection (Tsingtao, China), and animal experiments were performed according to the Guiding Principles for the Care and Use of Experiment Animals in Ocean University of China. The study protocol was reviewed and approved by the Institutional Animal Care and Use Committee, Ocean University of China, China. After the removal of hair using an animal hair clipper, the skins were excised from the abdominal part of the rats anesthetized with excessive ether, and then the residual subcutaneous fat adhering on the dermis side was wiped with scalpel and isopropyl alcohol until the skin was about 1 mm thick, followed by washing in PBS, pH 7.4. The rat skin was stored frozen at −20 °C after cutting into 4 cm^2 patches. Before performing the adhesion tests, the rat skin was thawed at 25 °C for 1 h and water was removed from the surface of the rat skin using a tissue paper.[42]

2.5.2 Microscopic observation of microneedles and skin insertion. Nano-microneedle: two different needle lengths (75 μm and 150 μm) of solid nano-microneedles (Fig. 3B and C) were used in this study.[38] The solid nano-microneedle was fabricated by dry and wet etching from silicon wafers, provided by Natong Bio-Nano Technology Co., Ltd. (Suzhou, China). These microneedles were examined using a stereomicroscope (P6000, Nikon) and a scanning electron microscope (SEM, Pro-X, Phenom). The electron microscope parameters are as follows: both the resolution of backscatter electron images and secondary electron image were 8 nm, the acceleration voltage was 5–15 kV, the magnification of the microscope was 20–150000 times and the filament category was cerium hexaborate.

Each microneedle array has 36 needles of 75/150 μm length in an area of 3 mm × 3 mm (Batch No. NT20160540). The array was fixed onto a supporting column (1 cm in diameter) of the applicator (MESO MASTER, Natong Bio-Nano), which provided insertion force of nearly 2 N. Microneedle arrays were inserted into the skin with a constant vibration frequency for 20 s.[34]

To evaluate the *in vitro* skin insertion capability of the proposed nano-microneedles, different lengths of microneedles were inserted into the porcine cadaver skin using the applicator. The microneedle patch was fixed to the applicator and then inserted into the skin for 2 min. The microneedle insertion site on the skin surface was exposed to blue ink for 1 min to identify the stratum corneum perforation sites. Histological sections of the skin were then excised to determine the micropores and self-closing. The skin sections were analyzed using an inverted microscope (IX-71, Olympus, Tokyo, Japan).[43]

2.5.3 *In vitro* transdermal delivery of insulin. Permeation studies were carried out with unjacketed Franz diffusion cells having a 0.785 cm^2 diffusion area (Aibiot Technology, Ltd, Zhengzhou, China). The receptor compartment was filled with a PBS buffer solution (25 mL, pH 7.4), and was maintained at 37 °C by means of a water bath and continuously stirred at 400 rpm. The different microneedle arrays were manually pressed into rat skins and different groups of insulin-loaded NPs solutions were filled in the donor chamber for testing. Then, the full-thickness skins were clamped between the donor and receptor chambers of a vertical diffusion cell with the SC side in contact with the donor phase. The amount of essential insulin diffused through the rat skin was determined by removing aliquots of 200 μL from the receptor compartments using a syringe and immediately replacing the same volume of solution (kept at 37 °C). The samples were transferred to volumetric flasks and stored in a refrigerator until they were analyzed.[44]

Insulin was detected using reversed-phase HPLC, and all samples were filtered through an aqueous membrane filter (0.45 μm pore size) before injection. All experiments were carried out in triplicate, and the results of these experiments dictated the microneedle lengths and NPs selected for the following experiment. Cumulative corrections were made to obtain the total amount of insulin permeated at each time interval.[45] The permeation rates of insulin at a steady state through skins were calculated from the slope of the linear portion of the cumulative amounts permeated through the skins per unit area *versus* time plot; cumulative amounts of insulin (Q) were calculated as follows:

$$Q = \left(C_n \times V + \sum_{i=1}^{n-1} C_i \times 0.5 \right) \Big/ S \tag{3}$$

Q represents the cumulative penetration, S the effective diffusion area, V the volume of the receiving liquid in the receiving chamber, C_i the concentration of insulin in the receiving liquid from the first time to the last sampling, and C_n the concentration of insulin in the receiving liquid at the time of sampling.

2.6 *In vivo* hypoglycemic studies

2.6.1 Diabetic animal model. Male SD rats (36 in total, 8 weeks old, 250 g) used in this study were acclimatized in the animal facility for two weeks before the experiment. The diabetic model was induced in rats with streptozotocin (45 mg kg^{-1} in citrate buffer, pH 4.0) administered by intraperitoneal injection. Rats were fasted overnight, but had free access to water prior to this experiment. Rats were deemed to be diabetic when their baseline glucose levels exceeded 16.7 mM after 48 h. Blood glucose levels were measured with a glucose assay kit using a Blood Analyzer (ONETOUCH® Ultra TM, China). Blood glucose levels were allowed to stabilize for one week.[46]

2.6.2 Blood glucose testing. The diabetic rats were selected for *in vivo* hypoglycemic studies and were divided in 4 groups containing six rats each as follows: (a) the microneedle of 150 μm length to promote the insulin-loaded CCA-NP transdermal delivery; (b) the microneedle of 150 μm length to promote free insulin transdermal delivery; (c) free insulin transdermal delivery; and (d) insulin subcutaneous injection using a hypodermic needle, which also served as a positive control group.[4] The concentrations of the insulin solution in four groups were 200 IU mL^{-1}.

The abdomen skin surface where the hairs were removed 24 h previously was washed using cotton soaked with 75% ethanol, after the SD rats were anesthetized with intraperitoneal injections of 60 mg kg^{-1} sodium pentobarbital. Before application of the nano-microneedle, the blood glucose values were detected to establish the baseline glucose levels. Then, microchannels were fabricated on the surface of the skin using the microneedle of 150 μm length, with an area of 1.0 cm^2 and a duration of 1 min. A 1.0 cm^2 × 0.5 cm cotton piece was then placed on the treated skin and 1 mL insulin-loaded NPs dissolved in a PBS solution was added to form the insulin patch. It was covered with a thin plastic film to prevent any leakage of the insulin solution. Blood samples were withdrawn from the tail vein at 0, 1, 2, 4, 6 and 8 h after the beginning of the experiments, and the blood glucose levels were measured.[46]

2.7 Statistical analysis

All data are expressed as mean ± SD. Data were analyzed statistically by using the SPSS 11.5 programs software package. Chemical structures are drawn using the ChemBioDraw Ultra 12.0 software. *$P < 0.05$ was regarded as significant and **$P < 0.01$ was considered as very significant.

3. Results and discussion

3.1 Synthesis of amphiphilic polymers and characteristics of self-aggregated nanoparticles based on polymers

The amphiphilic polymer CLA–CMCS (Fig. 1A and B) used in this work bears a hydrophilic CMCS[47] polysaccharide skeleton and a hydrophobic CLA group bridged *via* an ester bond.[48] The CLA–CMCS–Arg copolymer was obtained *via* the formation of an amide bond from amine-functionalized Arg (Fig. 1A and B) in the next step.[36] The incorporation of hydrophobic CLA groups renders the derived CC and CCA amphiphilic, enabling the

formation of nanoparticles in the aqueous solution.[49] The peaks at 1591 cm^{-1}, 1414 cm^{-1} and 2928 cm^{-1} are all characteristic peaks of CMCS, assigned to the stretching vibrations of C=O and CH$_2$COO– and the tensile vibration of C–H separately. The augmented peak at 1736 cm^{-1} corresponding to the stretching vibration of C=O group indicated the existence of the C=O group of a newly formed ester bond in the CC polymer and an escalated peak at 1640 cm^{-1} stands for the CO stretching vibration and indicated the formation of an amide bond linkage between Arg and CMCS (Fig. 1B).[39] Furthermore, four different conjugates (CC1, CC2, CCAa and CCAb) were prepared by varying the feed ratio of CLA and L-Arg to CMCS (Table 1).

By the ultrasonic self-assembly method,[50] CC/CCA polymers could easily form nanocarriers, as revealed by transmission electron microscopic (TEM) imaging and dynamic light-scattering (DLS) analysis (Fig. 1C and 2A). As presented in the TEM image, the resulting CC1/CCAa-NPs had spherical shapes with mono-disperse size [polydispersity index (PDI): 0.272 ± 0.02 and 0.252 ± 0.26] (Table 1). The average diameter of NPs was determined as 200 nm by DLS, which is consistent with the TEM observation. In addition, the toxicity of CC1/CCAa-NP to L929 cells was assessed by the MTT method. The cell viability of all groups were above 80% when the concentrations increased from 250 to 1500 μg mL^{-1} (Fig. 2C and D), which demonstrated that CC/CCA-NPs were nontoxic in a suitable concentration range.

3.2 Amphiphilic polymer-based nanoparticles encapsulate insulin with high drug payload

We further investigated EE and DL of the INS-loaded NPs based on different polymers. The maximal EE and DL could be attained up to 83.78 ± 3.73 and 34.72 ± 1.93% (Table 1). This high loading capacity can stem from the unique molecular structure of CCAa, a large amount of hydrophobic oleoresin attached to the hydrophilic polysaccharide skeleton, which generates micelles with low-density hydrophobic cores large enough to accommodate considerable amounts of insulin payloads.[51] In addition, an increase in the particle size also provides a larger surface area to carry more insulin.

Moreover, it is noteworthy that INS:CC/CCA-NPs were slightly larger in size than the empty NPs, as evidenced by both TEM image and DLS analysis (Fig. 3). This size difference could be reasonably ascribed to the expansion of particles required to accommodate insulin within the hydrophobic core to reach high loading (Fig. 1C). It confirmed that INS-loaded NPs still exhibited a spherical core/shell architecture, and insulin was predominantly entrapped in the hydrophobic core of the micelle. The increase in its inner hydrophobic core to accommodate high INS payload and the addition of insulin molecules will result in a slightly larger size of microspheres.[41]

3.3 Microscopic observation of nano-microneedles and microchannels

The SC was the barrier to the percutaneous penetration of drugs and breaking it required that the length of the microneedles were longer than the thickness of the stratum corneum (at least
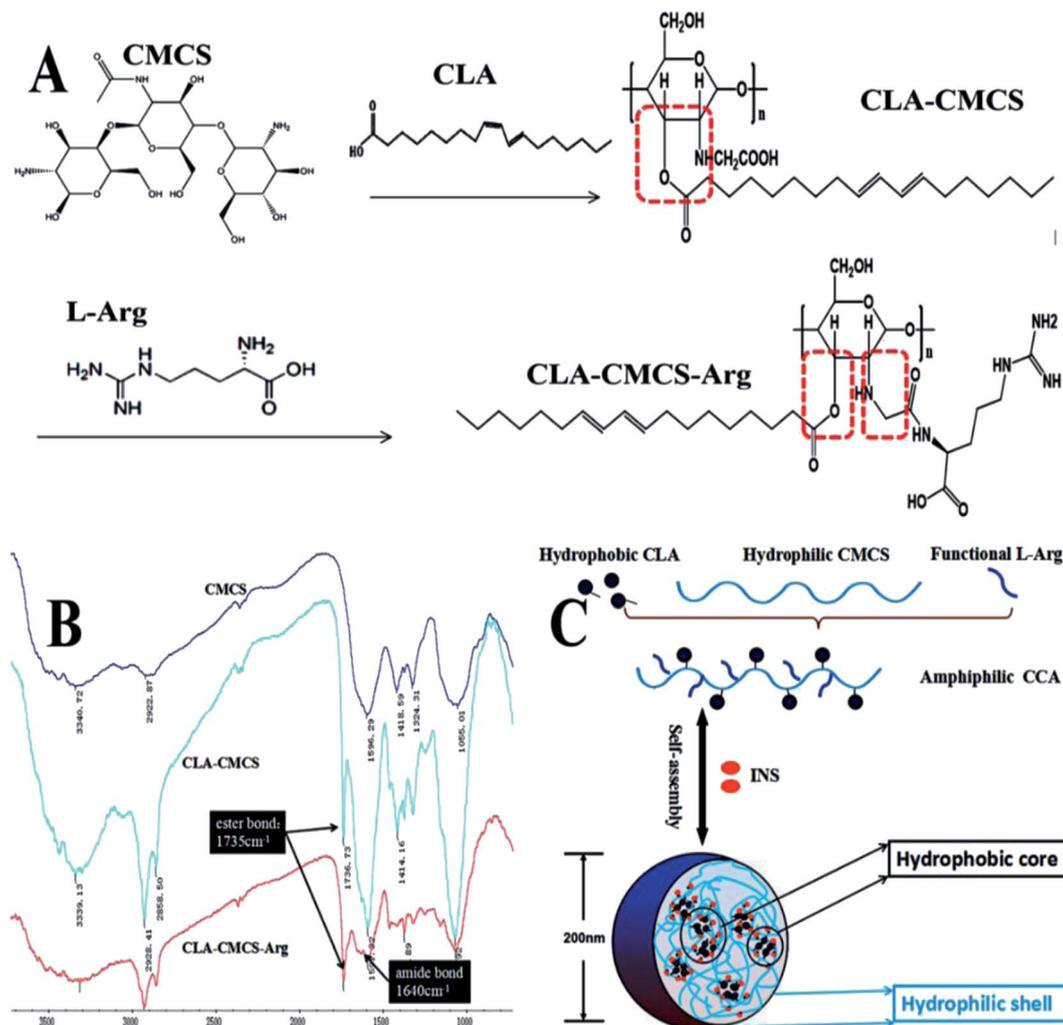
Fig. 1 (A) Schematic of CLA–CMCS and CLA–CMCS–Arg synthesis; (B) FT-IR spectra of CC/CCA polymers; and (C) CC/CCA polymers self-assemble into nanoparticles.

50 μm).[19] To address this problem, we used the small out-of-plane nano-microneedle arrays fabricated by a micro-fabrication technology (MEMS), and these short microneedles were sufficiently long to pierce the SC but short enough not to stimulate nerves in deeper tissues.[38] Fig. 4A shows a micrograph of the nano-microneedle arrays, which were uniform in size with very sharp tips. The lengths of the microneedle were 75 μm (short) and 150 μm (long) and sufficient to penetrate the stratum corneum and enter the active epidermis (Fig. 4A–C).

Each needle array has 36 needles on a 3 mm × 3 mm surface; other parameters were described in the above-mentioned method.

The nano-microneedle could be directly removed after the skin treatment without any biohazardous substances or degradation waste remains in the microchannel. In order to confirm the formation of microchannels in the skin, microneedles of 150 μm length were used with an applicator to pierce the skin at a constant speed. As shown in Fig. 4D and E, 36 micropores

Table 1 General properties of CC/CCA conjugates in distilled water

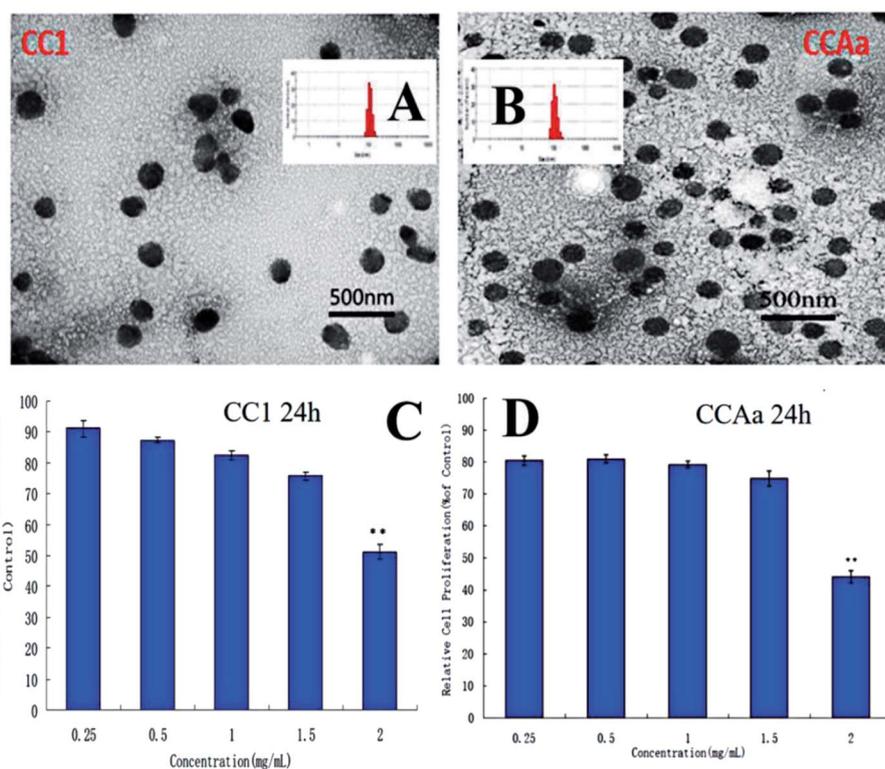| Samples | Components weight (g) | | | Mean size (nm) | PDI | EE (%) | DL (%) |
	CLA	CMCS	Arg				
CC1	0.25	1.00	—	196.4 ± 5.49	0.272 ± 0.02	75.26 ± 6.22	27.86 ± 3.12
CC2	1.00	1.00	—	155.3 ± 4.62	0.202 ± 0.13	81.26 ± 4.05	30.81 ± 2.67
CCAa	0.25	1.00	0.25	203.4 ± 3.42	0.252 ± 0.26	83.78 ± 3.73	34.72 ± 1.93
CCAb	0.25	1.00	1.00	229.4 ± 1.83	0.230 ± 0.19	79.72 ± 7.46	32.62 ± 4.72

Fig. 2 (A) and (B) TEM of CC1 and CCAa nanoparticles, respectively; (C) and (D) effects of CC1/CCAa–NPs on the proliferation ability of L929 cells (24 h), respectively. Note: **$P < 0.01$: 2 mg mL^{-1} vs. other concentrations.

were formed on the skin surface after the needle application with a pore diameter of 80 μm and a hole-to-hole spacing of 200 μm, and bleeding and erythema did not appear in the skin treated with the microneedle. In addition, H&E staining results also confirmed that the microneedles could effectively penetrate the SC and the microchannels on the skin created by the microneedles rapidly recovered within 2 h postadministration, as shown in Fig. 4F. These results indicated that nano-microneedles could penetrate the SC to create a large number of microchannels and maintain the large size of the micropore for a certain period of time, and finally, promote the penetration of insulin-loaded NPs or free insulin through the skin.

3.4 Effect of different nanoparticles on insulin permeation in vitro

As shown in Fig. 5A, we used insulin-loaded NPs based on different polymers for enhancing the transdermal delivery of insulin, and the CC/CCA-NPs were expected to provide a significant synergetic effect of penetrating the SC for increasing the transdermal efficiency of insulin.[52] The in vitro permeation rates of insulin from various nanoparticles are shown in Fig. 5B. The permeation rates of CC1-NPs, CC2-NPs, CCAa-NPs and CCAb-NPs were 3.18 ± 0.51, 2.77 ± 0.64, 6.56 ± 0.79, and 10.73 ± 1.47 μg (cm^{-2} h^{-1}), respectively. The permeation rates of insulin from CCA-NPs were increased 2.1–3.6 fold when compared with those not functionalized by arginine (Fig. 5B). CCAb-NPs had
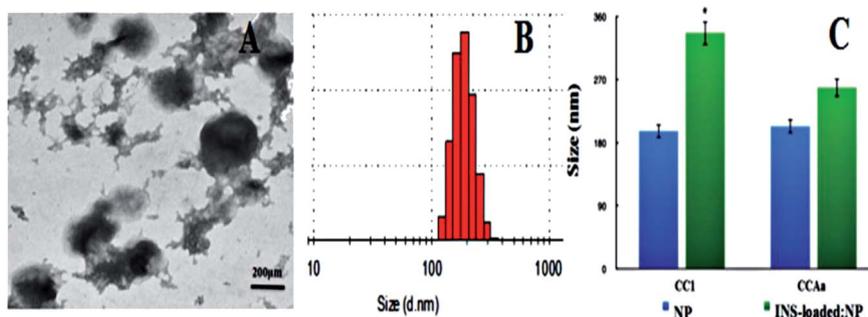

Fig. 3 (A) and (B) TEM and DLS of INS:CCAa–NPs, respectively; (C) changes in the size of CC1/CCAa–NPs after encapsulated insulin (blue: blank nanoparticles, green: INS-loaded nanoparticles). Note: *$P < 0.05$ vs. control; **$P < 0.01$ vs. control.
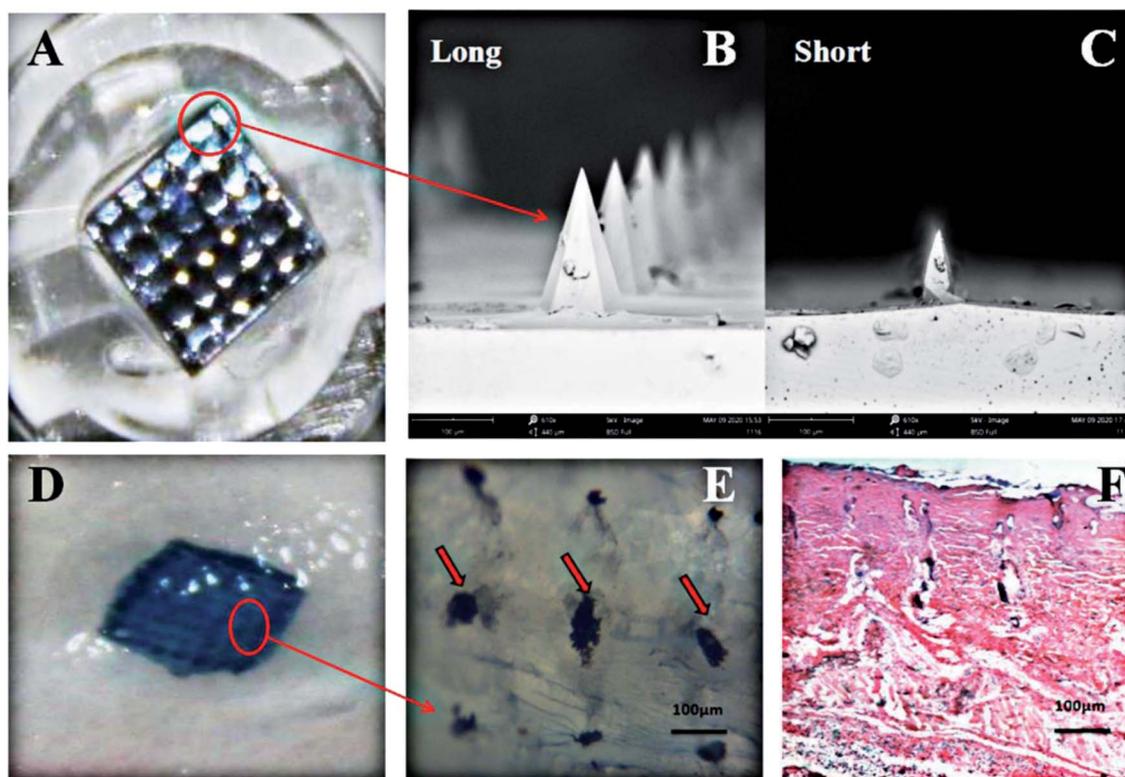
Fig. 4 Microscopic observation of microneedles and microchannels. (A) Nano-microneedles patch; (B) and (C) different lengths of microneedles; (D) and (E) microchannels on the skin after microneedle treatment; and (F) histological image of the skin after microneedle (long) treatment (2 h).

the highest permeation rate of 11.05 ± 1.45 μg (cm^{-2} h^{-1}). These results indicated that the nanoparticles could improve the diffusion coefficient of insulin due to the passive penetration and electrostatic interaction between skins and nanovesicles.[53] The Arg functional group and small size of the nanoparticles could enhance the fluidity of the lipid layer and the hydrophilic region in the SC, promote the transdermal rate of the particles, and then improve the penetration of INS. However, free INS exhibited a hexamer form (Fig. 5A) in the PBS solution (pH 7.4) with a large particle size, and it was difficult to penetrate the SC skin barrier without external force promoting penetration.[54] In addition, the permeation rate of nanoparticles
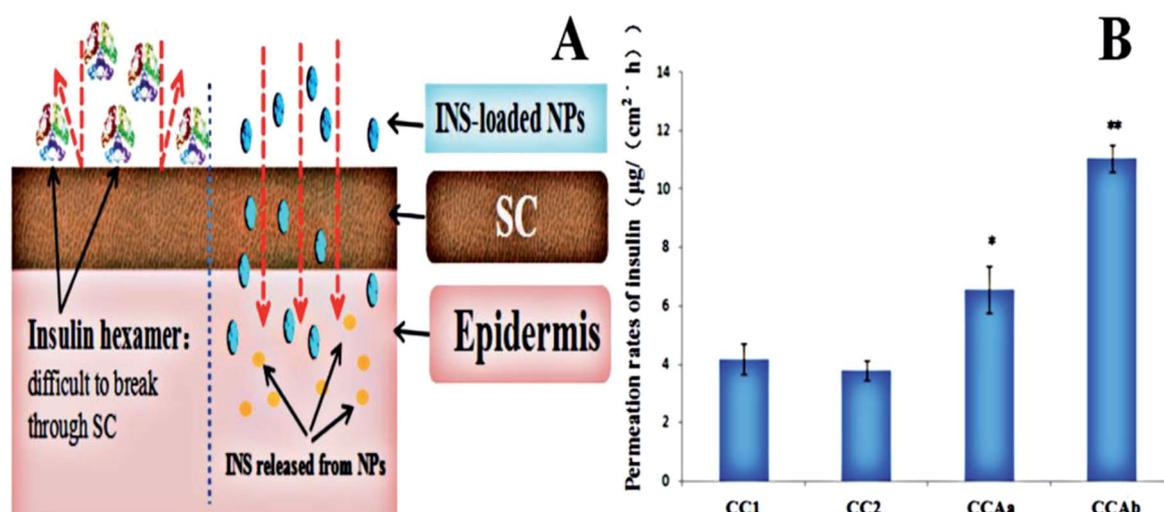

Fig. 5 (A) Schematic of transdermal delivery of insulin-loaded NPs and free insulin and (B) permeation rates of INS from different nanoparticles. Note: *$P < 0.05$ vs. control; **$P < 0.01$ vs. control.
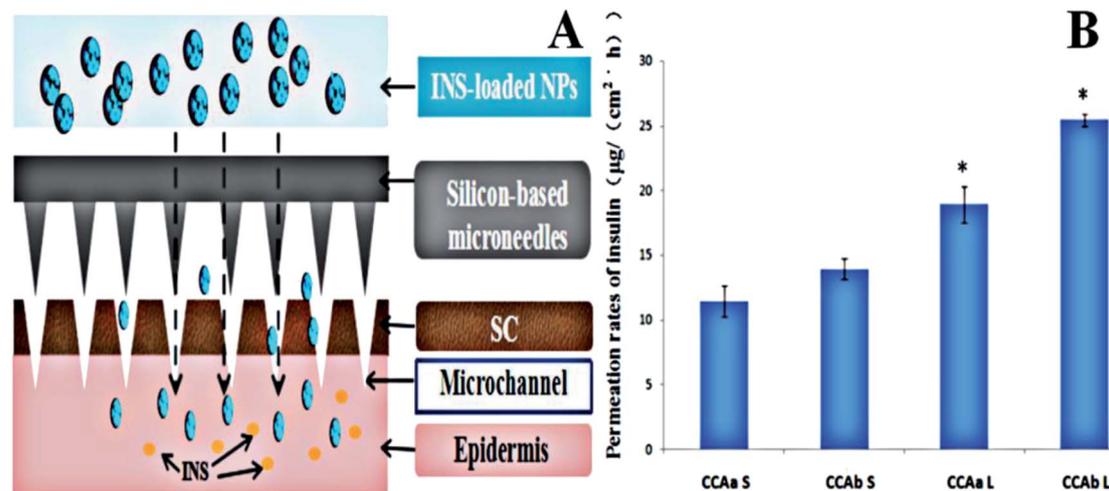
Fig. 6 Permeation rates of INS from different nanoparticles with different microneedles. (A) Schematic of the transdermal delivery of insulin-loaded NPs using a silicon-based microneedles system and (B) effect of the length of the microneedle (L and S) on insulin permeation. Note: *$P <$ 0.05 vs. control; **$P < 0.01$ vs. control.

showed little changes with the increase in particle size, which indicated that the particle size had little effects on the permeation rate under the condition of passive diffusion.

3.5 Effect of nanoparticle combination with microneedles on insulin permeation *in vitro*

We further presented an active strategy for enhancing the transdermal delivery of insulin using insulin-loaded CCA-NPs combined with microchannels pretreated by nano-microneedles (Fig. 6A). To assess whether nano-microneedle pretreatment resulted in an increased skin transport of the drug, the permeabilities of insulin through untreated and microneedle-treated rat skins were compared. The passive flux of insulin-loaded CCAb-NPs across untreated skins was $11.05 \pm 1.45\ \mu g\,(cm^{-2}\,h^{-1})$, as shown in Fig. 5B. After microneedle (long) treatment, the flux increased to $25.46 \pm 0.58\ \mu g\,(cm^{-2}\,h^{-1})$, an enhancement of more than 2.5-fold (Fig. 6B). Microneedle pretreatment significantly enhanced the penetration of insulin through the skin.[42] In addition, the results also indicated that the increase in the length of microneedles could enhance the
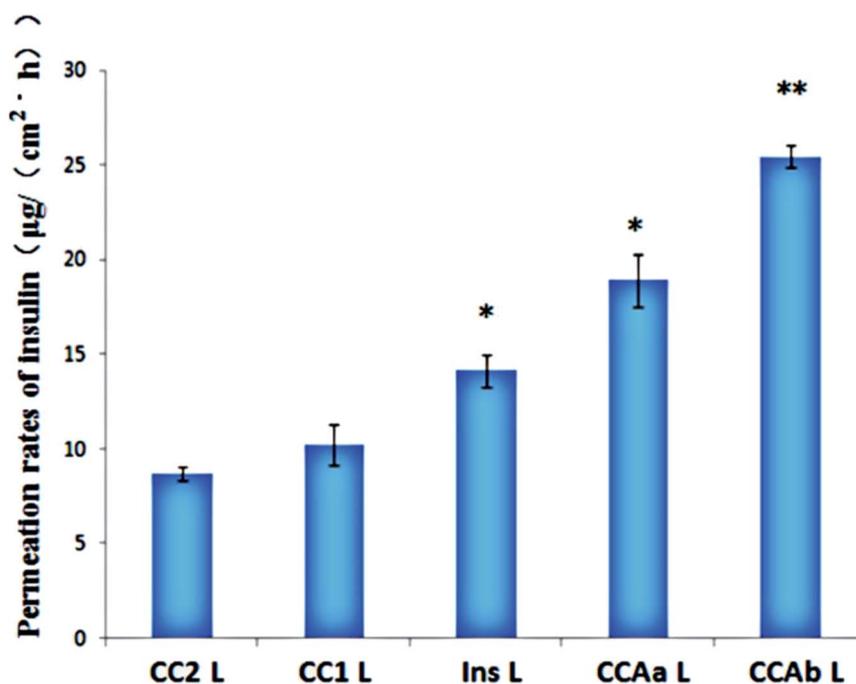

Fig. 7 Permeation rates of INS from different nanoparticles through the microneedle (L). Note: *$P < 0.05$ vs. control; **$P < 0.01$ vs. control.
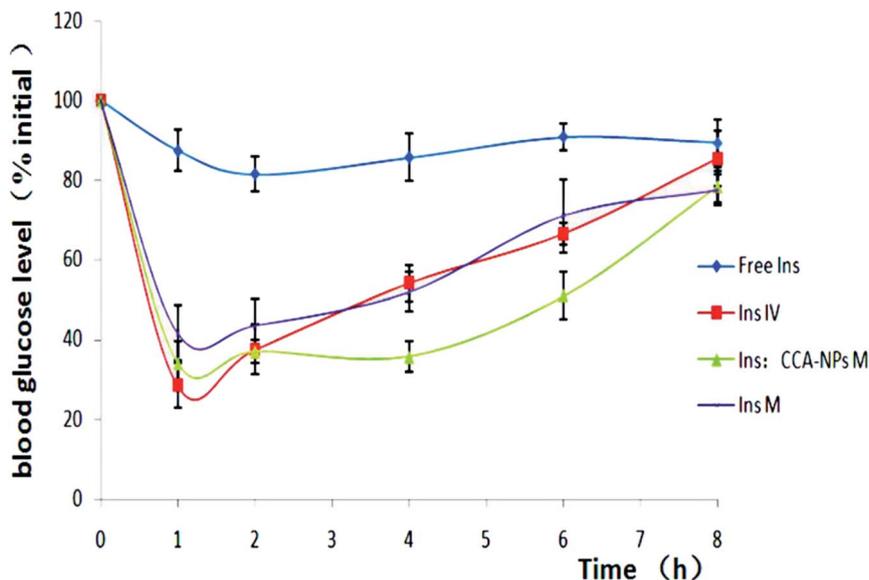
Fig. 8 Changes in blood glucose levels in rats as determined using passive delivery across untreated skin (◆), insulin injected intravenously (■), CCA-NPs combined with MNs (▲) and free insulin under the action of MN penetration (×). Data are presented as average values ± S.D.; $n = 6$.

penetration rate of the drug (Fig. 6B), mainly because the longer pretreated microchannels were easier to reach the dermis.

The microchannels effectively reduced the SC barrier and contributed to the increase in the diffusion coefficient of insulin, which resulted in a significant increase in the permeation rates. Obviously, the transdermal rate of free insulin under the action of microneedle penetration was 14.16 ± 0.85 μg (cm^{-2} h^{-1}), while it could not penetrate the SC *via* passive diffusion (Fig. 7). The permeation rates of insulin from CCAb-NPs combined with long microneedles were increased 2.5-fold and 1.1-fold when compared with those not functionalized with arginine and free insulin. In summary, the combination of functional nanoparticles and long microneedles resulted in a more powerful ability to enhance the permeation rates of insulin.[55]

3.6 Transdermal delivery of insulin to diabetic rats *in vivo*

To assess the *in vivo* efficacy of the combination scheme for diabetes treatment, the streptozotocin-induced type 2 diabetic rats were grouped as follows: transcutaneously exposed to free insulin, insulin injected by intravenous, insulin-loaded CCAb-NPs combined with MNs, and free insulin under the action of MNs penetration. The insulin dose applied for each rat was 45 mg kg^{-1}. As shown in Fig. 8, the group in which free insulin was applied to the untreated skin showed almost no hypoglycemic effect, confirming the well-known inefficiency of passive insulin delivery *via* the transdermal route.[56] The subcutaneous injection of insulin resulted in a rapid decrease in blood glucose levels; however, the blood glucose level showed a significant increase after 1.5 h. The hypoglycemic effect of free insulin after nano-microneedle penetration is consistent with the intravenous injection group. This indicated that the nano-microneedle could increase the skin permeability to deliver physiologically

relevant amounts of pharmacologically active insulin. However, the change in blood glucose levels caused by the combination of CCA-NPs and nano-microneedle penetration continues to stabilize at a lower level for 6 h. Therefore, the combination scheme used in the experiment can not only rapidly reduce the blood sugar level by penetrating the SC barrier, but also maintain the long-term hypoglycemic effect *via* controlled release of nanoparticles.[57]

4. Conclusion

Among various insulin-delivery techniques, the microneedle-assisted non-invasive delivery is currently believed to be the most efficient method. Especially, the combination of nano-particles and microneedles is very attractive, which has attracted tremendous attention from both academia and clinical medicine. In this study, a facile and efficient method for the green synthesis of well-distributed spherical CC/CCA-NPs has been developed. These NPs prepared in a self-assembly way were uniform and stable in solution over a period of one month, and they enhance the encapsulation efficiency and transdermal delivery of insulin. In order to obtain higher permeation rates of insulin, we chose silicon-based microneedles (75/150 μm) to fabricate microchannels, providing sufficient channels for the transport of insulin-loaded NPs. This study demonstrated that the combination scheme is an attractive alternative for conventional hypodermic injection, and that it not only provides a convenient operation but also allows fast and efficient hypoglycemic control. CCA-NPs combined with solid microneedles can provide an efficient and painless transdermal insulin delivery system by offering controlled release and a self-administration option, construct a promising general route for the non-invasive delivery of many other drugs and hold great potential for future applications. Interestingly, some related

studies have shown that the maintenance of weight loss would be useful for the remission of type 2 diabetes;[58] thus, whether long-term micro-adipocytes will have an impact or not on blood glucose will be our further research direction.

Funding

Author contributions

C. G. L. conceived the concept, directed the research, analysed the results, and revised the manuscript. P. Z. and Y. Z performed the experiments, analysed the experimental results, wrote the manuscript and discussion for experiments.

Conflicts of interest

The authors declare that there is no conflict of interest.

References

1 T. Scully, *Nature*, 2012, **485**, S2.
2 S. Wild, G. Roglic, A. Green, R. Sicree and H. King, *Diabetes Care*, 2004, **27**, 1047.
3 B. Zinman, S. P. Marso, N. R. Poulter, S. S. Emerson, T. R. Pieber, R. E. Pratley, M. Lange, K. Brownfrandsen, A. Moses and A. M. O. Francisco, *Diabetologia*, 2017, 61.
4 Y. Jicheng, Y. Yuqi, Y. Yanqi, D. S. Rocco, S. Wujin, R. Davis, F. S. Ligler, J. B. Buse and G. Zhen, *Proc. Natl. Acad. Sci. U. S. A.*, 2015, **112**, 8260.
5 M. Alberti and Z. Zimmet, *Diabet. Med.*, 1998, **15**, 539.
6 Group UPDS, *Lancet*, 1998, **352**, 854.
7 C. Mancusi, G. D. Simone, L. G. Best, W. Wang, Y. Zhang, M. J. Roman, E. T. Lee, B. V. Howard and R. B. Devereux, *Diabetes Care*, 2019, **55**, 87.
8 B. T. Allen, E. R. Delong and J. R. Feussner, *Diabetes Care*, 1990, **13**, 1044–1050.
9 T. Kuno, H. Tasaki and S. Miyazaki, *Acta Paediatr. Jpn. Overseas Ed.*, 2015, **38**, 464.
10 A. H. Barnett, B. Charbonnel, M. Donovan, D. Fleming and R. Chen, *Curr. Med. Res. Opin.*, 2012, **28**, 513.
11 M. Mata-Cases, D. Mauricio and J. F. Nadal, *J. Diabetes*, 2017, **9**, 34.
12 M. Kutlu, G. Aydoğan, F. Susuz and A. Ozata, *Diabetes Technol. Ther.*, 2006, **8**, 369.
13 J. Yu, Y. Zhang, J. Wang, D. Wen, A. R. Kahkoska, J. B. Buse and Z. Gu, *Nano Res.*, 2018, **12**, 1539.
14 A. Krauland, V. Leitner, V. Grabovac and A. Bernkop-Schnurch, *J. Pharm. Sci.*, 2010, **95**, 2463.
15 G. Bernstein, *Drug Dev. Res.*, 2010, **67**, 597.
16 R. Alany, *Pharm. Dev. Technol.*, 2018, **23**, 217.
17 J. Yu, Y. Zhang and Z. Gu, *Methods Mol. Biol.*, 2017, **1570**, 251.
18 M. R. Prausnitz and R. Langer, *Nat. Biotechnol.*, 2008, **26**, 1261.
19 K. Y. Seong, M. S. Seo, D. Y. Hwang, E. D. O'Cearbhaill, S. Sreenan, J. M. Karp and S. Y. Yang, *J. Controlled Release*, 2017, 265.
20 S. Mitragotri, D. Blankschtein and R. Langer, *Science*, 1995, **269**, 850.
21 I. C. Lee, Y.-C. Wu, S.-W. Tsai, C.-H. Chen and M.-H. Wu, *RSC Adv.*, 2017, 7, 5067–5075.
22 B. Xu, G. Jiang, W. Yu, D. Liu, Z. Yang, J. Zhou, S. Sun, Y. Liu, B. Xu and G. Jiang, *J. Mater. Chem. B*, 2017, **41**, 8200.
23 R. Rastogi, S. Anand and V. Koul, *Drug Dev. Ind. Pharm.*, 2010, **36**, 1303–1311.
24 M. Higaki, M. Kameyama, M. Udagawa, Y. Ueno, Y. Yamaguchi, R. Igarashi, T. Ishihara and Y. Mizushima, *Diabetes Technol. Ther.*, 2006, **8**, 369.
25 L. Hong, D. Han, M.-X. Li, P. Zhang and C.-G. Liu, *Int. J. Cosmet. Sci.*, 2017, **39**, 337.
26 M. García-Díaz, C. Foged and H. M. Nielsen, *Int. J. Pharm.*, 2015, **482**, 84.
27 M. Marimuthu, D. Bennet and S. Kim, *Polym. J.*, 2013, **45**, 202.
28 M. R. Prausnitz, *Adv. Drug Delivery Rev.*, 2004, **56**, 581.
29 S. Khan, M. U. Minhas, I. A. Tekko, R. F. Donnelly and R. R. S. Thakur, *Drug Delivery and Translational Research*, 2019.
30 Y. C. Kim, J. H. Park and M. R. Prausnitz, *Adv. Drug Delivery Rev.*, 2012, **64**, 1547.
31 T. M. Blicharz, G. Ping, B. M. Bunner, L. L. Chu, K. M. Leonard, J. A. Wakefield, R. E. Williams, M. Dadgar, C. A. Tagliabue and R. E. Khaja, *Nat. Biomed. Eng.*, 2018, **2**, 151.
32 M. C. Chen, K. Y. Lai, M. H. Ling and C. W. Lin, *Acta Biomater.*, 2018, **65**, 66.
33 S. Liu, M. N. Jin, Y. S. Quan, F. Kamiyama, H. Katsumi, T. Sakane and A. Yamamoto, *J. Controlled Release*, 2012, **161**, 933.
34 W. Martanto, S. P. Davis, N. J. Holiday, H. S. Gill and M. R. Prausnitz, *Pharm. Res.*, 2004, **21**, 947.
35 S. Zhang, Y. Qiu and Y. Gao, *Acta Pharm. Sin. B*, 2014, **4**, 100.
36 P. Zhang, H. X. Guo and C. G. Liu, *Polymers*, 2020, **12**, 408.
37 C. Edens, M. L. Collins, J. L. Goodson, P. A. Rota and M. R. Prausnitz, *Vaccine*, 2015, **33**, 4712.
38 Y. Tao, Y. Miao, T. Wu, J. Liu, X. Yang, X. Bai, L. Dan and B. Zhou, *Chin. J. Dermatovenereol. Integr. Tradit. West. Med.*, 2017, **16**, 11.
39 P. Zhang, S. R. Zhao, Y. Y. Yao, H. Wang, Y. Yang and C. G. Liu, *Molecules*, 2019, **24**, 555.
40 K. Akiyoshi, S. Deguchi, N. Moriguchi, S. Yamaguchi and J. Sunamoto, *Macromolecules*, 1993, **26**, 3062.
41 W. Tuo, C. Chao, L. Juan, L. Cheng, P. Paola, L. Xiaoxuan, C. Qiang, H. Shuaidong, L. Zicai and F. Maurizio, *Proc. Natl. Acad. Sci. U. S. A.*, 2015, **112**, 2978.

42 K. Y. Seong, M. S. Seo, D. Y. Hwang, E. D. O'Cearbhaill, S. Sreenan, J. M. Karp and S. Y. Yang, *J. Controlled Release*, 2017, **265**, 48.

43 S. Zhang, Y. Qiu and Y. Gao, *Acta Pharm. Sin. B*, 2014, **4**, 100–104.

44 M.-H. Ling and M.-C. Chen, *Acta Biomater.*, 2013, **9**, 8952–8961.

45 Y. Xie, B. Xu and Y. Gao, *Nanomedicine*, 2005, **1**, 184.

46 H. Chen, H. Zhu, J. Zheng, D. Mou, J. Wan, J. Zhang, T. Shi, Y. Zhao, H. Xu and X. Yang, *J. Controlled Release*, 2009, **139**, 63.

47 C. P. Zhou, Y. L. Liu, H. L. Wang, P. X. Zhang and J. L. Zhang, *Int. J. Pharm.*, 2010, **392**, 127.

48 Y. Li, S. Zhang, X. Meng, X. Chen and G. Ren, *Carbohydr. Polym.*, 2011, **83**, 130.

49 C. G. Liu, X. G. Chen and H. J. Park, *Carbohydr. Polym.*, 2005, **62**, 293.

50 C. Li, C. C. Tho, D. Galaktionova, X. Chen and U. Mirsaidov, *Nanoscale*, 2019, 11.

51 M. P. Conte, J. K. Sahoo, Y. M. Abul-Haija, L. Kha and R. V. Ulijn, *ACS Appl. Mater. Interfaces*, 2018, **10**, 3069.

52 J. L. Wu, C. G. Liu and Z. H. Huang, *J. Mater. Sci.: Mater. Med.*, 2012, **23**, 1921.

53 M. Qindeel, N. Ahmed, F. Sabir, S. Khan and A. Ur-Rehman, *Drug Dev. Ind. Pharm.*, 2019, **45**, 1.

54 X. Zhao, Y. Zu, S. C. Zu, D. Wang, Y. Zhang and B. Zu, *Drug Dev. Ind. Pharm.*, 2010, **36**, 1177.

55 M. Dathe, K. Gast, D. Zirwer, H. Welfle and B. Mehlis, *Chem. Biol. Drug Des.*, 2010, **36**, 344.

56 H. G. Kim, D. L. Gater and Y. C. Kim, *Drug Delivery Transl. Res.*, 2018, **8**, 281.

57 M. Haga, M. Akatani, J. Kikuchi, Y. Ueno and M. Hayashi, *J. Controlled Release*, 1997, **43**, 139.

58 M. E. Lean, W. S. Leslie, A. C. Barnes, N. Brosnahan, G. Thom, L. Mccombie, C. Peters, S. Zhyzhneuskaya, A. Al-Mrabeh and K. G. Hollingsworth, *Lancet*, 2018, **391**, 541.